Heavy ellipsoids in creeping shear flow: Transitions of the particle rotation rate and orbit shape

Fredrik Lundell and Allan Carlsson*
Linné FLOW Centre, KTH Mechanics, Royal Institute of Technology, 100 44 Stockholm, Sweden
(Received 8 September 2009; revised manuscript received 9 December 2009; published 29 January 2010)

The motion of an inertial ellipsoid in a creeping linear shear flow of a Newtonian fluid is studied numerically. This constitutes a fundamental system that is used as a basis for simulations and analysis of flows with heavy nonspherical particles. The torque on the ellipsoid is given analytically by Jeffery [Proc. R. Soc. London, Ser. A **102**, 161 (1922)]. This torque is coupled with the angular-momentum equation for the particle. The motion is then governed by the Stokes number $\mathrm{St}=\rho_e\dot{\gamma}l^2/\mu$, where ρ_e is the density of the ellipsoid, $\dot{\gamma}$ is the rate of shear, l is the length of the major axis of the ellipsoid, and μ is the dynamic viscosity of the fluid. For low St (the numerical value depends on the aspect ratio of the particle), the particle motion is similar to the Jeffery orbits obtained for inertia-free particles with the addition of an orbit drift so that the particle eventually lies in the flow-gradient plane. At higher St, more drastic effects are seen. For particles oriented in the flow-gradient plane, the rotation rate increases rather abruptly to half the shear rate in a narrow range of St. For particles with other orientations, the motion goes from a kayaking motion to rotation around an oblique axis. It is suggested that, depending on aspect and density ratios, particle inertia might be sufficient to explain and model orbit drift observed previously at low Reynolds numbers. It is discussed how and when the assumption of negligible fluid inertia and strong particle inertia can be justified from a fundamental perspective for particles of different aspect ratios.

DOI: 10.1103/PhysRevE.81.016323 PACS number(s): 47.15.G−, 47.55.Kf

I. INTRODUCTION

Flows in which elongated or platelike particles are suspended in a Newtonian fluid occur in many engineering and biological systems. To indicate the width of applications, papermaking [1–4], aerosols [5,6], coating systems [7,8], or particle motion in the respiratory system [9,10] can be mentioned. Thus, the motion of elongated particles in different flow situations are necessary to model (i) the rheology of such suspensions [11,12] and (ii) the motion and orientation of individual particles in a flow [3,13–15]. In the second case, the aim might be, e.g., to understand and develop a manufacturing process or predict medical consequences. Note that for particles in gas flows, the density ratio between the particle and the liquid is typically of the order of 1000. In water, typical density ratios are 1–10. The present work is aimed at particles in Newtonian fluids, and the results reviewed and cited reflect this restriction.

The basis for such modeling is the motion of single particles in simplified flow situations. As the modeling ability is steadily increasing, this research area has noted considerable attention and many aspects of these motions have been studied with a wide variety of methods, experimental as well as numerical [16–26]. Further on, the results necessary to set the present work in perspective will be summarized in more detail.

The particular case studied here is an inertial ellipsoid in linear creeping shear flow. The situation under study is depicted in Fig. 1. The ellipsoid is defined by

$$x^2+\frac{y^2}{k_b^2}+\frac{z^2}{k_c^2}=\left(\frac{l}{2}\right)^2.$$

Thus, k_b and k_c are the aspect ratios of the ellipsoid and l a measure of its size. Primed quantities refer to an inertial reference frame and quantities without primes refer to a body-fixed coordinate system. The ellipsoid is put in a shear flow given by $u'=\dot{\gamma}y'$ where $\dot{\gamma}$ is the rate of shear. The orientation of a spheroid ($k_b=k_c$) is defined by the angles φ (the angle between the x' axis and the projection of the x axis on the $x'y'$ plane) and θ (the angle between the z' and x axes). The Reynolds number based on shear is here defined as $\mathrm{Re}_{\dot{\gamma}}=\dot{\gamma}l^2/\nu$, where ν is the kinematic viscosity of the fluid. All analysis in this paper is based on the creeping-flow assumption, i.e., $\mathrm{Re}_{\dot{\gamma}}=0$. Thus, the results are a corner stone when it comes to phenomenological understanding of motions of heavy particles at low $\mathrm{Re}_{\dot{\gamma}}$. Furthermore, it will be argued that, for heavy particles, the assumption of $\mathrm{Re}_{\dot{\gamma}}=0$ can give quantitative agreement up to $\mathrm{Re}_{\dot{\gamma}}=1$ or more for certain aspects of the particle motion.

Jeffery [27] determined the torque on an ellipsoidal particle in an unbounded linearly varying Stokes flow (Reynolds number zero). He gives analytical expressions for the torque given the flow, fluid viscosity and lengths of the ellipsoid axes together with the orientation and angular velocity vector of the particle. Furthermore, he determined the rotational motion of light (where light means that particle inertia is negligible) spheroids by setting the torque to zero and solve for the angular velocities. He showed that the spheroid undergoes a periodic motion around the vorticity axis (the z' axis in Fig. 1) in one of an infinite number of closed orbits (usually called *Jeffery orbits*) somewhat similar to the motion of a kayak paddle. His results are routinely used as a starting point in studies of a fundamental nature and when

*Present address: Department of Mechanical Engineering, University of British Columbia, Vancouver, British Columbia V6T 1Z4, Canada.

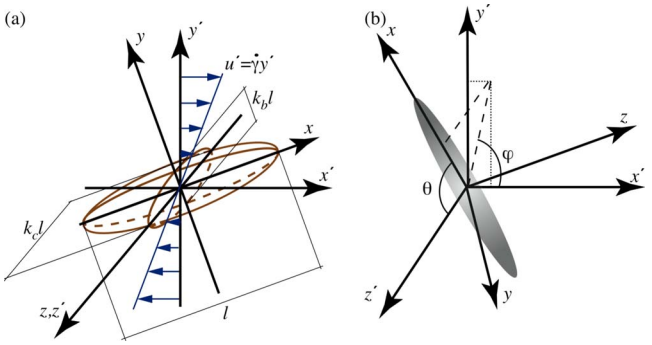

FIG. 1. (Color online) Physical situation under study in (a) and definition of the angles θ and φ for an oriented spheroid in (b).

flows with elongated particles are modeled [19,21,22,25,28].

In a Jeffery orbit, a light spheroid with $k_b=k_c<1$ spends most of the time around $\varphi=0$ and π. Periodically, the spheroid flips between these two values of ϕ and during this flipping, the angle θ will vary, unless it is $\pi/2$. If time is scaled with $\dot{\gamma}$, the period and $\varphi(t)$ were obtained by Jeffery [27] as

$$T_J = 2\pi\left(\frac{1}{k_b^2}+1\right)k_b, \quad \cot\varphi = -\frac{1}{k_b}\cot\left(\frac{2\pi t}{T_J}+\varphi_0\right),$$

where φ_0 is a phase defined by the initial orientation. The relation between φ and θ is defined by the orbit parameter

$$C = \frac{1}{k_b}\tan\theta\left(\frac{1}{k_b^2}\sin^2\varphi+\cos^2\varphi\right)^{0.5}.$$

The orbit parameter ranges from 0 to ∞ and the extremes correspond to constant $\theta=0$ and $\theta=\pi/2$, respectively. Here, this span is transformed to [0,1] by introducing $C_B=C/(C+1)$. For light particles in creeping flow (i.e., $\mathrm{Re}_{\dot{\gamma}}=0$, Stokes flow) the orbit parameter is constant in time and is defined by the initial orientation of the particle. If the Reynolds number is nonzero, there are effects of fluid inertia. There are also effects of the inertia of the particle, which are measured by the Stokes number, here defined as $\mathrm{St}=\kappa\,\mathrm{Re}_{\dot{\gamma}}$, where $\kappa=\rho_e/\rho_f$ where ρ_e and ρ_f are the densities of the particle and fluid, respectively. The effects of fluid and particle inertia have recently been given considerable attention. Nonzero *particle* inertia [17,23,25] (i) gives a drift so that the longest axis ultimately is in the flow-gradient plane and (ii) increases the rate of flipping. The orientation drift and decrease of rotation period is due to the fact that inertia resists deceleration as the main axis of the particle approaches and moves through the flow-vorticity plane. Furthermore, it has been shown [22,29] that also weak *fluid* inertia tends to drift slender bodies to flipping in the flow-gradient plane. The period of rotation *increases* with $\mathrm{Re}_{\dot{\gamma}}$ and eventually the particle ceases to rotate at a critical $\mathrm{Re}_{\dot{\gamma}}$. Similar effects have also been reported in simulations of buoyant ellipsoids [19], where the critical $\mathrm{Re}_{\dot{\gamma}}$ (at which rotation stops) is increased with an increasing κ. Neutrally buoyant particles ($\kappa=1$, i.e., $\mathrm{Re}_{\dot{\gamma}}=\mathrm{St}$) have been studied numerically [21,24] and it has been found that for small $\mathrm{Re}_{\dot{\gamma}}$ a prolate spheroid ($k_b=k_c=0.5$) finally rotates around the *minor* axis, which then is aligned with the vorticity axis. At higher Reynolds numbers, the asymptotical orientation changes drastically and the spheroid ends up with the *major* axis aligned with the direction of vorticity. A full understanding of the effect of fluid and particle inertia on the orientation and rotation period for different particle aspect ratios is yet to be established.

In this paper, the torque on an ellipsoid in creeping shear flow ($\mathrm{Re}_{\dot{\gamma}}=0$) given by Jeffery [27] will be coupled with the equations of motion of the ellipsoid. The magnitude of particle inertia will be increased considerably compared to previous studies and drastic effects are predicted at high St. The present results are of course relevant in gas flows with small nonspherical particles (low Reynolds number, high density-ratio) but it will be argued that it might also be important at lower density ratios if the aspect ratio is moderate.

We will first study rotation when one axis of the ellipsoid is fixed and aligned with the vorticity axis ($\theta=\pi/2$). This initial analysis is followed by modeling and analyses of the full three-dimensional rotation. These sections start with stating the governing equations and thereafter the results are presented and discussed briefly. A section with a discussion on how the results could be verified in a physical experiment follows. In Sec. V, two specific consequences of the present results are discussed: (i) implications on particle dynamics in the Re/St plane and (ii) how particles will migrate when the shear is combined with gravity/sedimentation. Finally, the conclusions are summarized.

II. ROTATION AROUND THE VORTICITY AXIS

A. Governing equations

The law of angular momentum for rotation around one (fixed) axis is $M_z=I_z\ddot{\varphi}$, where I_z is the moment of inertia of the ellipsoid and dots indicate differentiation with respect to time. With the nondimensional time being $t=t^*\dot{\gamma}$ (t^* is the dimensional time), the equation of motion for the ellipsoid rotating around the z-axis, with Jeffery's expression for M_z, is found to be

$$\mathrm{St}\frac{k_c(k_bK_\alpha+K_\beta)}{20}\ddot{\varphi} = \frac{1-k_b^2}{1+k_b^2}\left(\frac{1}{2}-\sin^2\varphi\right)-\left(\frac{1}{2}+\dot{\varphi}\right) \quad (1)$$

where $K_\alpha=K(k_b^2,k_c^2)$, $K_\beta=K(k_b^{-2},k_c^2k_b^{-2})$, and

$$K(C_1,C_2) = \int_0^\infty \frac{d\lambda}{(1+\lambda)\{(1+\lambda)(C_1+\lambda)(C_2+\lambda)\}^{1/2}}.$$

For $\mathrm{St}=0$, this is of course equal to Jeffery's equation for rotation around the z axis.

B. Results

Equation (1) was integrated numerically [with $K(C_1,C_2)$ determined by the software package Mathematical] to give φ as a function of time. The initial condition was chosen to be $\varphi=\dot{\varphi}=0$. In Fig. 2(a), the angle φ is shown as a function of t for an ellipsoid with $k_b=k_c=0.1$ and two values of St, 0.01 and 10 000. For small St, the left-hand side of Eq. (1) is close to zero and the well-known solution of Jeffery is obtained. The ellipsoid spends most of the time close to $\varphi=N\pi$, where N is an integer, and flips quickly with a period

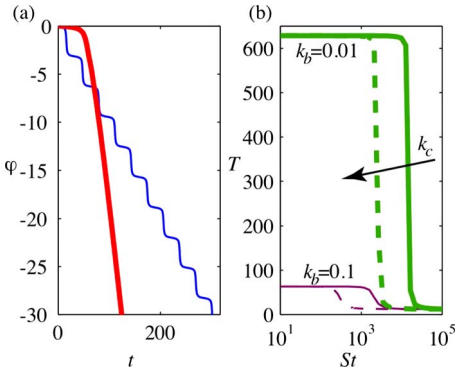

FIG. 2. (Color online) (a) Rotation angle φ as a function of time for $k_b=k_c=0.1$ and St=0.1 (blue, thin), and St=1000 (red, thick). (b) Rotation period T as a function of St for $k_b=0.01$ (green, thick) and $k_b=0.1$ (purple, thin) and $k_c=0.01$ and $k_c=0.1$ (solid and dashed, respectively).

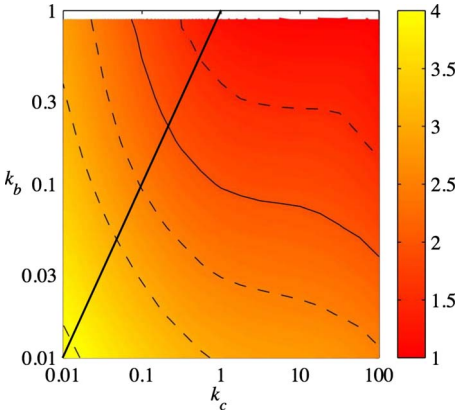

FIG. 3. (Color online) Contours of the logarithm of $St_{0.5}$ as a function of k_b and k_c. The solid contour is 100 and the dashed contours are $10^{1.5}$, $10^{2.5}$, 10^3, and $10^{3.5}$. The thick solid line shows the line $k_b=k_c$, which indicates prolate spheroids.

for a full rotation of T_J. For St=10 000, on the other hand, there is an initial transient and later, φ increases linearly with time (the ellipsoid rotates with a constant angular velocity). This constant angular velocity is given by the fact that the angular acceleration of increasingly heavy particles will approach zero. The angular velocity is then given by the value of $\dot{\varphi}$ that satisfies

$$\int_0^{2\pi} M_z(\varphi,\dot{\varphi})d\varphi = 0,$$

where $M_z(\varphi,\dot{\varphi})$ is given analytically from Jeffery [27] [the φ dependence is the same as the right-hand side of Eq. (1)]. This gives the expected result for the rotation rate and period T_H of heavy particles,

$$\dot{\varphi} = -0.5, \quad T_H = 4\pi.$$

Thus, the period of rotation (after initial transients) must decrease from T_J to T_H as St is increased. In Fig. 2(b), the period of rotation T is shown as a function of St for four aspect-ratio combinations. For each case, there is a sharp transition, increasingly so with reduced k_b, from T_J (which varies with k_b) to 4π at a distinct range of St. The critical value of St is different for the different aspect-ratio combinations. In Fig. 3, contours of the logarithm of the transitional Stokes number $St_{0.5}$, defined as the Stokes number at which $T=(T_J+T_H)/2$, is shown for varying k_b and k_c. The critical Stokes number is seen to decrease with both k_b and k_c.

It can actually be demonstrated numerically that $St_{0.5}$ occurs when

$$St_{0.5}\frac{k_c(k_bK_\alpha + K_\beta)}{20} = 0.8, \tag{2}$$

i.e., by the lumped parameter in the left-hand side of Eq. (1) [35]. Thus, $St_{0.5}$ is easily calculated for a given ellipsoid.

III. ROTATION IN THREE DIMENSIONS

It has previously been observed that particle inertia gives a drift toward the state of rotation studied in Sec. II. We will now study three-dimensional rotation for a wide range of St. The formulation below is valid for all ellipsoids. For the present scope, results for prolate spheroids will be presented. In all calculations, the initial condition was $\varphi=0$, $\theta=\theta_0$. The value of θ_0 is indicated in the figure captions.

A. Governing equations

Shivarama and Fahrenthold [30] derived a constraint-free quaternion-based formulation of the equations of motion for a rotating (and translating) body and the rotation part of this formulation will be used below. The orientation of a body is now described by a quaternion, i.e., a vector of four numbers with norm 1,

$$\mathbf{e} = [e_0 \quad e_1 \quad e_2 \quad e_3]^T. \tag{3}$$

The physical interpretation of the quaternion is that if the body has been rotated by an angle ψ around an axis defined by a unit vector in the inertial frame of reference, $\mathbf{b}'=[b_1' \quad b_2' \quad b_3']$, the corresponding quaternion is

$$\mathbf{e} = [\cos(\psi/2) \quad b_1'\sin(\psi/2) \quad b_2'\sin(\psi/2) \quad b_3'\sin(\psi/2)].$$

The rotation matrix $\mathbf{R}$ relating a vector $\mathbf{a}'$ in the inertial system to the components in the body-fixed system, $\mathbf{a}$ (i.e., $\mathbf{a}'=\mathbf{Ra}$), is then

$$\mathbf{R} = \mathbf{E}\mathbf{G}^T, \tag{4}$$

where

$$\mathbf{E} = \begin{bmatrix} -e_1 & e_0 & -e_3 & e_2 \\ -e_2 & e_3 & e_0 & -e_1 \\ -e_3 & -e_2 & e_1 & e_0 \end{bmatrix} \tag{5}$$

and

$$\mathbf{G} = \begin{bmatrix} -e_1 & e_0 & e_3 & -e_2 \\ -e_2 & -e_3 & e_0 & e_1 \\ -e_3 & e_2 & -e_1 & e_0 \end{bmatrix}. \tag{6}$$

Now introduce the angular-momentum vector $\mathbf{h}=\mathbf{J}\omega$, where $\mathbf{J}$ and ω are the moment-of-inertia matrix and rotational ve-

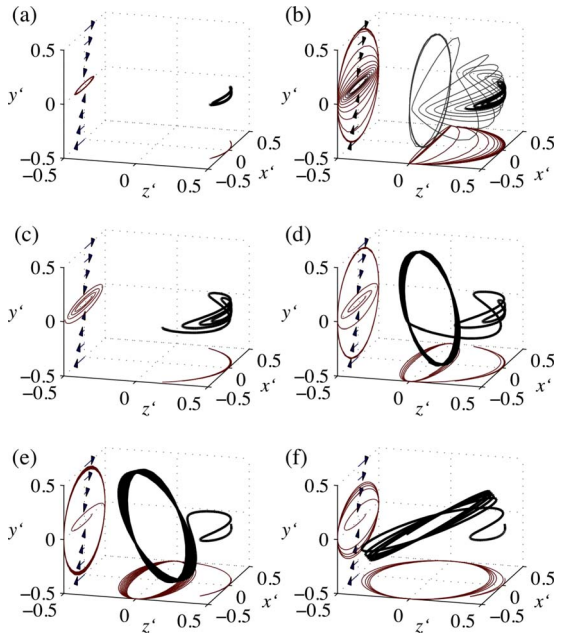

FIG. 4. (Color online) Trajectory of the spheroid end point (thick black) and its projection on the $x'y'$ and $x'z'$ planes (red, thin). $k_b=k_c=0.1$, $\theta_0=\pi/8$ and St=100, 316, 562, 1000, 3162, and 10 000 from (a) to (f). Time goes from 0 to 225, except for (b) where the thinner gray extension of the trajectory shows the motion up to $t=800$.

locity vector, respectively, in the body-fixed coordinates. The nondimensional equations of motion for an ellipsoid in creeping shear can then be written as

$$\dot{\mathbf{e}} = \frac{1}{2}\mathbf{G}^T\omega, \quad \dot{\mathbf{h}} = -\mathbf{\Omega}\mathbf{h} + \frac{16\pi}{3\mathrm{St}}\mathbf{T}, \tag{7}$$

where $\mathbf{\Omega}=2\mathbf{G}\dot{\mathbf{G}}^T$ and $16\pi\mathbf{T}/3\mathrm{St}$ is the nondimensional torque, obtained from Jeffery [27],

$$\mathbf{T} = \begin{bmatrix} (K_\beta k_b + K_\gamma k_c)^{-1}[(k_b^2 - k_c^2)D_{2,3} + (k_b^2 + k_c^2)(V_{2,3} - \omega_1)] \\ (K_\gamma k_c + K_\alpha)^{-1}[(k_c^2 - 1)D_{3,1} + (k_c^2 + 1)(V_{3,1} - \omega_2)] \\ (K_\alpha + K_\beta k_b)^{-1}[(1 - k_b^2)D_{1,2} + (1 + k_b^2)(V_{1,2} - \omega_3)] \end{bmatrix}. \tag{8}$$

where $K_\gamma=K(k_c^{-2},k_b^2k_c^{-2})$ and $\mathbf{D}$ and $\mathbf{V}$ are the rates of deformation and vorticity in the body-fixed system.

B. Results

1. Motion of a prolate spheroid for various St and initial orientations

Equation (7) can be integrated numerically to yield the orientation [in terms of $\mathbf{e}$, which then gives the rotation matrix $\mathbf{R}$ via Eq. (4)] of the ellipsoid as a function of time. Results for $k_b=k_c=0.1$ will be reported. In Fig. 4, the end-point trajectory is shown as a function of time for increasing values of St in Figs. 4(a)–4(f). Time goes from 0 to 225 [in Fig. 4(b), the trajectory up to $t=800$ is shown as a thinner, gray line). The projection of the end point on the $x'y'$ and $x'z'$ planes are shown and the shear is indicated with arrows. For St=100 in Fig. 4(a), the end point is seen to move in an almost closed circuit, similar to the Jeffery orbit at which it was initiated. This means that the orbit parameter C_B is close to constant. As St is increased, the end point is seen to spiral outwards, i.e., C_B is increasing. In Fig. 4(b), it is clearly seen that this spiraling continues until the particle is rotating around the vorticity axis.

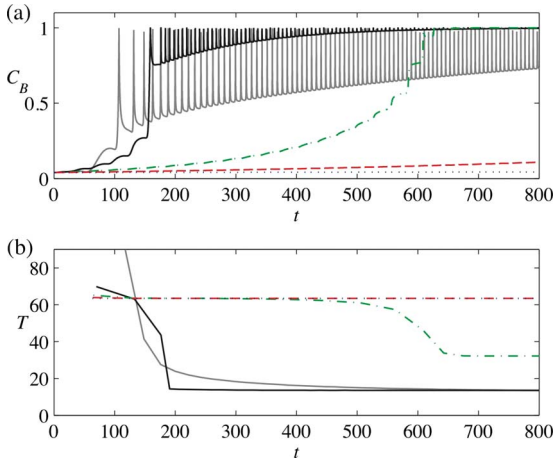

FIG. 5. (Color online) (a) Orbit parameter C_B and (b) rotation period T as a function of time. St=10 (blue, dotted), 100 (red, dashed), 316 (green, dash-dotted), 1000 (black, solid), and 10 000 (gray, solid).

At even higher Stokes numbers, a more dramatic approach to this rotation is seen. At St=1000, Fig. 4(d), the end point is seen to do two rounds of spiraling before inertia takes the end point over to $z'<0$ and the spheroid rotates around a *tilted* axis, which is in the $y'z'$-plane. As time increases, this axis approaches the z' axis slowly. In Figs. 4(e) and 4(f), it is seen that both the maximum angle and the direction of this tilt is a function of St. Animations of St =100, 1000, and 10 000 as well as three different initial conditions are provided digitally [31].

Since the particles do not stay in a single Jeffery orbit forever, the value of the orbit parameter C_B will vary. C_B as a function of time for the trajectories in Figs. 4(a), 4(b), 4(d), and 4(e) is shown in Fig. 5(a). At low St (dotted and dash-dotted curves) the particle rotation is still qualitatively similar to that described by the analysis of Jeffery [27] and C_B is only increasing very slowly. At intermediate values, there is a close to monotonous approach to $C_B=1$ (dash) whereas at high St, C_B oscillates between 1 and a minimum value for every half period since the tilted rotation is fundamentally different from the Jeffery orbits.

As the axis of rotation approaches the z' axis, the minimum value of C_B is seen to increase. The period of rotation [as shown in (b)] is seen to be long (T_J) at low St. For the intermediate case it is long at first and somewhere in between T_J and T_H once the particle has reached $C_B=1$ (this final rotation period is the one studied in Sec. II). Once started, a heavy particle has a period not too far from T_H, but when the axis of rotation is tilted, the rotation period is somewhat longer than T_H (albeit shorter than T_J).

The effect of the initial condition will also be illustrated. In Fig. 6, the end-point trajectory is shown for St=1000 and

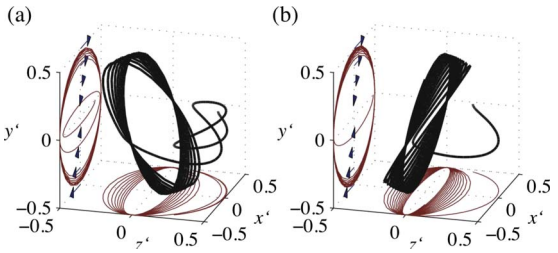

FIG. 6. (Color online) Trajectory of the spheroid end point (black, thick) and its projection on the $x'y'$- and $x'z'$-planes (red, thin). $k_b=k_c=0.1$. (a) and (b) St=1000, $\theta_0=3\pi/8$, and $\pi/4$. Time goes from 0 to 225.

$\theta_0=\pi/4$ and $3\pi/8$; $\theta_0=\pi/8$ for the same St is shown in Fig. 4(d). Both the absolute angle and direction of the tilt during the transient toward $C_B=1$ is seen to depend on the initial condition. In Fig. 7(a) C_B is shown as a function of time for St=1000 and $\theta_0=\pi/8$, $\pi/4$, and $3\pi/8$. The time before the tilted rotation starts is of course higher for low θ_0 than for higher. However, the angle of the tilted axis with respect to vorticity, at the instant when the particle enters the tilted rotation, is varying in amplitude (and direction) with θ_0. As before, the rotation period is quite long until the particle has reached the state of tilted rotation and in this state, it is close to T_H [see Fig. 7(b)].

Figure 7(c) shows the time it takes for the minimum value of C_B during one rotation to reach 0.99, denoted t_{99}. The curves show t_{99}/T_J as a function of St for $k_b=k_c=0.316$ (thin) and 0.1 (thick) for different initial conditions $\theta_0=\pi/8$, $\pi/4$, and $3\pi/8$ (solid, dashed and dash-dotted, respectively). The transitional Stokes number for fixed rotation around the vorticity axis, $\mathrm{St}_{0.5}$, is indicated with vertical dashed lines. The exact value of t_{99} is seen to depend on the initial condition, but the range of St for which it is small is similar for a given ellipsoid geometry. Furthermore, the minimum of t_{99} is seen to be close to $\mathrm{St}_{0.5}$.

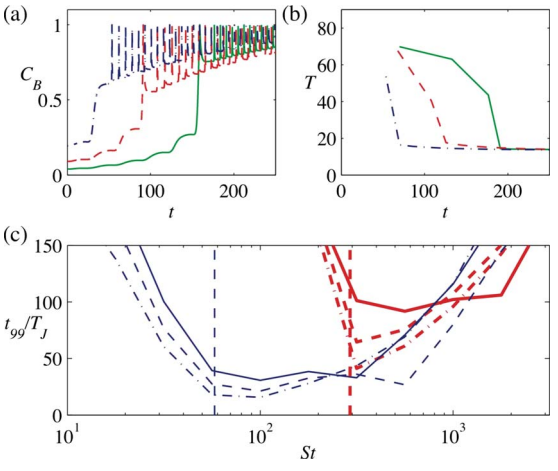

FIG. 7. (Color online) (a) Orbit parameter C_B and (b) rotation period T as a function of time for St=1000, $\theta_0=\pi/8$ (green, solid), $\pi/4$ (red, dashed), and $3\pi/8$ (black, dash-dotted). (c) t_{99} for $k_b=k_c=0.3$ (blue, thin) and 0.1 (red, thick), $\theta_0=\pi/8$ (solid), $\pi/4$ (dashed), and $3\pi/8$ (dash-dotted). The vertical dashed lines indicate the value of $\mathrm{St}_{0.5}$ for the respective aspect ratio.

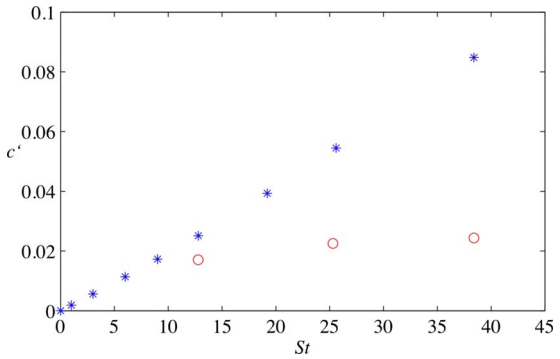

FIG. 8. (Color online) Orbit drift parameter c' as a function of St for the present case without fluid inertia (blue, *) and from simulations including fluid and particle inertia with $\kappa=1.001$ by Yu *et al.* [24] (red, ○). $k_b=k_c=0.5$.

2. Quantification of the orbit drift

The observed orbit drift, i.e., that the spheroid tends to go toward the orbit with $C_B=1$, can be quantified by the orbit drift parameter c' [24,32], defined as

$$c' = \frac{2\log(C_{\varphi=-\pi}/C_{\varphi=-2\pi})}{T_J}. \tag{9}$$

In Fig. 8 the orbit drift parameter is shown as a function of St for prolate spheroids with aspect ratio $2(k_b=k_c=0.5)$. The present data are shown as stars (blue online). The circles (red online) are values obtained from Yu *et al.* [24] for a nearly neutrally buoyant particle ($\kappa=1.001$) in fully inertial (fluid as well as particle) simulations. In these simulations, the Reynolds number is approximately equal to St since the density ratio is almost 1.

For high St, it is clear that the present simulations with only particle inertia strongly overpredicts the orbit drift. In fact, Yu *et al.* [24] reported that the orbit drift changes direction toward lower C at $\mathrm{Re}\approx 160$. However, the orbit drift at Re=12.8 is of the same order in our case and theirs. Unfortunately, no fully inertial data has been found for even lower Re, but a possible implementation of the results in Fig. 8 is that at low Re, perhaps 5 or lower, particle inertia is the dominant cause of the orbit drift in this particular case.

IV. POSSIBILITY OF EXPERIMENTAL VERIFICATION

In order for the results above to be verified experimentally, one must set up an experiment where the Stokes number is in the range of $\mathrm{St}_{0.5}$ and the Reynolds number is low enough so that the torques given by Jeffery [27] (creeping flow) is a good approximation of the torques on the ellipsoid. Furthermore, the effects of sedimentation under gravity must be small. One way to obtain such conditions experimentally would be to use a Couette flow apparatus with two walls moving in the opposite directions. Such a setup has been used previously for experimental studies of particle rotation [20,33]. In between these walls, a shear flow will be at hand. A limited number of particles could be added and their motion tracked with cameras. Of course, the particles will move

with the flow and/or due to gravity depending on parameters. However, if the Couette apparatus is designed carefully and the flow is in the direction of gravity, the translational velocity will be zero at some position between the walls. In this section, we will investigate the demands in terms of gravity, shear rate, particle size and particle density that arise if a certain Re-St combination is to be obtained.

The critical Stokes number is fairly high for most aspect ratios. Consequently, high-density ratios $\kappa=\rho_e/\rho_f$ are needed if these high Stokes numbers are to be reached while the Reynolds number is small. In an experimental context, this means that sedimentation becomes an important factor. However, if both the Reynolds number given by the shear $\mathrm{Re}_{\dot\gamma}$ and the sedimentation, $\mathrm{Re}_{sed}=U_{sed}l/\nu$, are small, the transition in rotation rate as well as orbit shape should be experimentally verifiable. This is possible since the equations for the flow are linear for Re=0. Consequently, flow fields (and the resulting forces on particles) can be superimposed. The flow due to the sedimentation can thus be added to the solution of Jeffery and the effects modeled by Eq. (1) will be present.

The sedimentation Reynolds number can be calculated from the sedimentation velocity, U_{sed}. From the force on an ellipsoid in pure translation [34], the sedimentation speed can be determined to be

$$U_{sed}=\frac{l^2k_bk_c(\rho_e-\rho_f)(X_0+K_g)a_g}{12\mu},$$

where

$$X_0=\int_0^\infty\frac{d\lambda}{\{(1+\lambda)(k_b+\lambda)(k_c+\lambda)\}^{1/2}},$$

and $K_g=K_\alpha$ or $K_g=K_\beta$ if gravity is along the x or y axis, respectively, and a_g is the acceleration of gravity.

Now, the physical limitations will be illustrated. Since κ must be large to reach $\mathrm{St}_{0.5}$, the assumption $\rho_e-\rho_f\approx\kappa\rho_f$ is valid. This gives

$$\mathrm{Re}_{sed}=\frac{U_{sed}l}{\nu}=\frac{l^3k_bk_c\kappa(X_0+K_g)a_g}{12\nu^2}.$$

In order for the creeping-flow approximation to be valid, both $\mathrm{Re}_{\dot\gamma}$ and Re_{sed} must be small. The necessary length and time scales can be determined as functions of fluid viscosity and gravity if the governing Reynolds numbers $\mathrm{Re}_{\dot\gamma}$ and Re_{sed} are assumed to be equal (it is straightforward to let them vary by a constant). This mutual Reynolds number must then be small in order for the assumptions to be valid. From $\mathrm{Re}=\mathrm{Re}_{\dot\gamma}=\mathrm{Re}_{sed}$ we get (after using $\kappa=\mathrm{St}\,\nu/\dot\gamma l^2$)

$$\frac{\dot\gamma^2l}{a_g}=\frac{k_bk_c\,\mathrm{St}(X_0+K_g)}{12}. \tag{10}$$

Note that $\mathrm{St}_{0.5}$ is a function of k_b and k_c as seen in Fig. 3 and that $\mathrm{St}_{0.5}$ would be the interesting region of St for an experiment. We introduce

$$f_\alpha(k_b,k_c)=\frac{k_bk_c\,\mathrm{St}_{0.5}(X_0+K_\alpha)}{12},$$

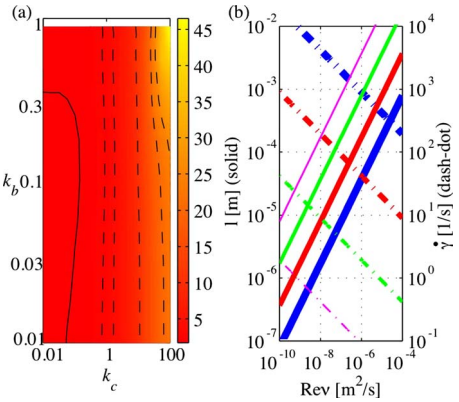

FIG. 9. (Color online) (a) The function $f_\alpha(k_b,k_c)$. Contours are 2 (solid), 3, 4, 10, 20, and 25. (b) l (solid) and $\dot\gamma$ (dash-dotted) for different levels magnitudes of a_g, from $a_g=g$ (blue, thick) to $a_g=10^{-6}g$ (purple, thin) where g is the gravitational acceleration on earth. The intermediate lines are $10^{-2}g$ and $10^{-4}g$.

$$f_\beta(k_b,k_c)=\frac{k_bk_c\,\mathrm{St}_{0.5}(X_0+K_\beta)}{12},$$

and f_α is shown in Fig. 9(a). Restricting ourselves to prolate spheroids $(k_b=k_c<1)$ computations show that $1\le f_\alpha/f_\beta<2.5$, thus they are of the same order of magnitude. It is therefore enough to consider f_α in the estimations below. From Eq. (10) and the definition of $\mathrm{Re}_{\dot\gamma}$, l and $\dot\gamma$ become

$$l=\frac{(\mathrm{Re}\,\nu)^{2/3}}{(f_\alpha a_g)^{1/3}},\quad \dot\gamma=\frac{(f_\alpha a_g)^{2/3}}{(\mathrm{Re}\,\nu)^{1/3}}$$

It is seen in Fig. 9(a) that our restriction gives a value of f_α around 2.5. The order of magnitude of l and $\dot\gamma$ will be estimated using this value. In Fig. 9(b), l and $\dot\gamma$ are shown as functions of Re ν (with $f_\alpha=2.5$). If the experiments are to be done in air with a particle size of the order of mm and Re $=0.01$ (Re $\nu\approx1.5e-7$), Fig. 9(b) shows that a gravity of $10^{-4}g$ (given by the second thinnest, green online, line) and a shear of around 3 s^{-1} is needed. Such conditions could be obtained in a sounding rocket experiment. The necessary density ratio is determined by Re and $\mathrm{St}_{0.5}(k_b,k_c)$. On earth (the thick, blue online, lines), micrometer sized particles would be necessary. An alternative interpretation of Fig. 9(b) is that it shows at what particle size and shear rate the transition from Jeffery's solution to the rotation at constant rotation rate will set in. In this context, it shows whether the transition will be relevant in a given application.

V. DISCUSSION

Even though the present analysis is strictly valid only for Re=0, the results give an indication of the particle motion at high density-ratios and low Reynolds numbers. The quantitative meaning of high density-ratios and low Reynolds numbers in this context is yet to be established. However, it is clear that the present effects will be a function of particle aspect ratio: for a given $\mathrm{Re}_{\dot\gamma}$, less slender particles will be affected by particle inertia at lower density ratios compared to more slender ones. Observe that Fig. 8 indicates that the

results can have importance up to surprisingly high Reynolds number and low density-ratios. Knowledge of the parameter regions [in terms of (i) density ratio or Stokes number, (ii) Reynolds number, and (iii) aspect ratio of the particle] where particle and/or fluid inertia are negligible is necessary in order to apply proper models for particle motion in simulations of suspensions. The possible choices are four: (i) neglect all inertia, (ii) neglect fluid inertia as in this study, (iii) neglect particle inertia, and (iv) neglect no inertia. So far, the overall literature contains only a sparse sampling of this parameter space.

Nevertheless, the results in Sec. II together with previous results show that there must be several regions in the $\mathrm{Re}_{\dot{\gamma}}/\mathrm{St}$ plane. Three of these are long period flipping as given by Jeffery (low $\mathrm{Re}_{\dot{\gamma}}$, low St), fast rotation (low $\mathrm{Re}_{\dot{\gamma}}$, high St) as found here and very slow or no rotation (high $\mathrm{Re}_{\dot{\gamma}}$; low St) [19,21,22]. The transition zones between these regions depend on k_b and k_c and are yet to be established. One fundamental question is how far from the St axis (Re=0) our results can be used as a phenomenological reference to understand the particle dynamics.

Our results also have implications on the motion of particles under influence of shear and gravity together. Broday *et al.* [17] reported that particle inertia together with gravity in the x' direction will give rise to a net migration in the y' direction at intermediate Stokes numbers. This migration occurs since (i) elongated particles sediment sideways when the direction of gravity is not normal or parallel to the particle director and (ii) the distribution function of φ becomes nonsymmetric at intermediate Stokes numbers. Our results in Sec. II imply that this migration will cease to exist at even higher values of St, since the particle then rotates with constant angular velocity and consequently, the distribution of φ is symmetric. Furthermore, the tilted orbits seen in Figs. 4 and 6 will give rise to a migration in the z' direction if there is gravity along y' while the axis of rotation is tilted. If gravity is pointing in the negative y' direction, this migration would be toward positive z' for the orbit in Fig. 6(a) and in the opposite direction for the orbit in Fig. 6(b).

VI. CONCLUSIONS

The effect of particle inertia on the motion of ellipsoids in creeping shear flow has been studied. This flow case is one of the four basic assumptions possible (the four cases are full inertia and neglecting particle and/or fluid inertia) when modeling suspension flows with nonspherical particles. The results are thus the basis for the understanding of particle motion and orientation of particles at low Reynolds numbers and high density-ratio.

The present assumptions are used in simulations since they have the advantage that the particle motion can be determined from a set of seven ordinary differential equations. Thus, there is no need of a numerical flow solver for the flow around the particles (since analytical expressions for the torque [27] are used). Even though the analysis is strictly valid only for Re=0, there are indications, both from literature and from the comparison with results from Yu *et al.* [24] in Fig. 8, that particle inertia alone might be sufficient to predict the orbit drift even at Re=1 or higher. Whether the assumption of zero fluid inertia is appropriate depends on the particle aspect ratio, Reynolds number and Stokes number and the full analysis of this parameter space is yet to be performed.

Furthermore, drastic changes of the particle motion at high St are predicted. These motions are fundamentally different from Jeffery orbits: the particle motion goes from kayaking or flipping to rotation around a fixed or almost fixed axis. These motions will be found in applications where the particle/fluid density ratio and shear rate are high enough for the Stokes number to be in the range of $\mathrm{St}_{0.5}$ while the Reynolds number is still small enough for fluid inertia to be neglected. An order-of-magnitude analysis shows that these motions can be verified experimentally under micro gravity conditions for very low Reynolds numbers (0.01 or lower). However, following the previous arguing they might well appear also at higher Reynolds numbers (order 1 or slightly higher). The last observation relaxes the demand of micro gravity for the experimental verification.

Technically, the detailed conclusions on the particle motion are:

(i) for fixed rotation around the vorticity axis, the rotation period (after initial transients) decreases from T_J to T_H in a distinct St interval around $\mathrm{St}_{0.5}$;

(ii) if the initial orientation of the major axis is not in the $x'z'$ plane ($C_B=1$), particle inertia induces a drift in the particle motion toward this plane;

(iii) the approach to $C_B=1$ is different for low and high values of St. For low Stokes numbers, C_B increases almost monotonously, whereas at high values of St rotation around a tilted axis (slowly moving toward the z' axis) occurs transiently.

(iv) The time it takes to reach $C_B>0.99$, t_{99}, depends on initial condition, aspect ratio and Stokes number. It has a minimum not far from $\mathrm{St}_{0.5}$ and increases with the slenderness of the particle.

ACKNOWLEDGMENTS

We are grateful for discussions with P. Henrik Alfredsson, Fritz Bark, Anders Dahlkild, Rebecca Lingwood, and L. Daniel Söderberg at KTH Mechanics. E. John Hinch at Cambridge University is gratefully acknowledged for pointing out the observation in Eq. (2). F.L. was supported by the Swedish Research Council; A.C. and F.L. were supported by the European Union FP6 project EcoTarget.

[1] J. A. Olson, I. Frigaard, C. Chan, and J. P. Hämäläinen, Int. J. Multiphase Flow **30**, 51 (2004).
[2] M. Parsheh, M. Brown, and C. Aidun, J. Fluid Mech. **545**, 245 (2005).
[3] S. B. Lindström and T. Uesaka, Phys. Fluids **19**, 113307 (2007).
[4] M. Hyensjö, A. Dahlkild, P. Krochak, J. Olson, and J. Hämäläinen, Nordic Pulp Pap. Res. J. **22**, 376 (2007).
[5] W. Holländer, Adv. Colloid Interface Sci. **46**, 49 (1993).
[6] L. Gradon, P. Grzybowski, and A. Podgorski, J. Aerosol Sci. **22**, S153 (1991).
[7] T.-C. Jen, L. Li, W. Cui, Q. Chen, and X. Zhang, Int. J. Heat Mass Transfer **48**, 4384 (2005).
[8] Z. Li, J. Zhu, and C. Zhang, Powder Technol. **150**, 155 (2005).
[9] Z. Zhang and C. Kleinstreuer, J. Comput. Phys. **198**, 178 (2004).
[10] G. Miserocchi, G. Sancini, F. Mantegazza, and G. Chiappino, Environ. Health **7**, 4 (2008).
[11] E. Guth and R. Simha, Colloid Polym. Sci. **74**, 147 (1936).
[12] C. J. S. Petrie, J. Non-Newtonian Fluid Mech. **87**, 369 (1999).
[13] J. Lin, X. Shi, and Z. Yu, Int. J. Multiphase Flow **29**, 1355 (2003).
[14] J. Lin, W. Zhang, and Z. Yu, J. Aerosol Sci. **35**, 63 (2004).
[15] P. H. Mortensen, H. I. Andersson, J. J. J. Gillissen, and B. J. Boersma, Int. J. Multiphase Flow **34**, 678 (2008).
[16] E. Gavze and M. Shapiro, J. Fluid Mech. **371**, 59 (1998).
[17] D. Broday, M. Fichman, M. Shapiro, and C. Gutfinger, Phys. Fluids **10**, 86 (1998).
[18] G. Rienacker and S. Hess, Physica. A **267**, 294 (1999).
[19] E.-J. Ding and C. K. Aidun, J. Fluid Mech. **423**, 317 (2000).
[20] C. Zettner and M. Yoda, J. Fluid Mech. **442**, 241-266 (2001).
[21] D. Qi and L.-S. Luo, J. Fluid Mech. **477**, 201-213 (2003).
[22] G. Subramanian and D. L. Koch, J. Fluid Mech. **535**, 383 (2005).
[23] G. Subramanian and D. L. Koch, J. Fluid Mech. **557**, 257 (2006).
[24] Z. Yu, N. Phan-Thien, and R. I. Tanner, Phys. Rev. E **76**, 026310 (2007).
[25] H. Altenbach, K. Naumenko, S. Pylypenko, and B. Renner, Z. Angew. Math. Mech. **87**, 81 (2007).
[26] X. K. Ku and J. Z. Lin, Phys. Scr. **80**, 025801 (2009).
[27] G. B. Jeffery, Proc. R. Soc. London, Ser. A **102**, 161 (1922).
[28] Y.-G. Tao, W. K. den Otter, and W. J. Briels, Phys. Rev. Lett. **95**, 237802 (2005).
[29] P. Saffman, J. Fluid Mech. **1**, 540 (1956).
[30] R. Shivarama and E. Fahrenthold, ASME J. Dyn. Syst., Meas., Control **126**, 124 (2004).
[31] See supplementary material at http://link.aps.org/supplemental/10.1103/PhysRevE.81.016323 for animations of the orbits in Figs. 4 and 6.
[32] A. Karnis, H. Goldsmith, and S. Mason, Can. J. Chem. Eng. **44**, 181 (1966).
[33] C. Zettner and M. Yoda, Exp. Fluids **30**, 346 (2001).
[34] H. Lamb, *Hydrodynamics* (Cambridge University Press, Cambridge, UK, 1997).
[35] This fact was pointed out for us by Hinch.